Boron-Proton Nuclear-Fusion Enhancement Induced in Boron-Doped Silicon Targets by Low-Contrast Pulsed Laser

A. Picciotto,[1,*] D. Margarone,[2,†] A. Velyhan,[2] P. Bellutti,[1] J. Krasa,[2] A. Szydlowsky,[3,4] G. Bertuccio,[5] Y. Shi,[5] A. Mangione,[6] J. Prokupek,[2,7] A. Malinowska,[4] E. Krousky,[8] J. Ullschmied,[8] L. Laska,[2] M. Kucharik,[7] and G. Korn[2]

[1]*Micro-Nano Facility, Fondazione Bruno Kessler, 38123 Trento, Italy*
[2]*Institute of Physics ASCR, v.v.i. (FZU), ELI-Beamlines Project, 182 21 Prague, Czech Republic*
[3]*Institute of Plasma Physics and Laser Microfusion, 01-497 Warsaw, Poland*
[4]*National Centre for Nuclear Research, 05-400 Otwock, Poland*
[5]*Politecnico di Milano, Department of Electronics Information and Bioengineering, 22100 Como, Italy*
[6]*Institute of Advanced Technologies, 91100 Trapani, Italy*
[7]*Czech Technical University in Prague, FNSPE, 115 19 Prague, Czech Republic*
[8]*Institute of Plasma Physics of the ASCR, PALS Laboratory, 182 00 Prague, Czech Republic*

(Received 12 January 2014; revised manuscript received 1 April 2014; published 19 August 2014)

We show that a spatially well-defined layer of boron dopants in a hydrogen-enriched silicon target allows the production of a high yield of alpha particles of around 10^9 per steradian using a nanosecond, low-contrast laser pulse with a nominal intensity of approximately 3×10^{16} W cm^{-2}. This result can be ascribed to the nature of the long laser-pulse interaction with the target and with the expanding plasma, as well as to the optimal target geometry and composition. The possibility of an impact on future applications such as nuclear fusion without production of neutron-induced radioactivity and compact ion accelerators is anticipated.

DOI: 10.1103/PhysRevX.4.031030 Subject Areas: Nuclear Physics, Plasma Physics

I. INTRODUCTION

The $^{11}\mathrm{B}(p,\alpha)2\alpha$ nuclear-fusion reaction was first studied in the 1930s by Oliphant and Rutherford [1]. Interest from the scientific community in this reaction is now increasing due to the possibility of producing energetic alpha particles without neutron generation, which may allow the building of an "ultraclean" nuclear-fusion reactor [2–4]. The first experimental demonstration of a laser-driven $^{11}\mathrm{B}(p,\alpha)2\alpha$ reaction was performed using the interaction of a high-intensity (around 2×10^{18} W cm^{-2}) picosecond laser pulse with a boron-enriched polymeric target. This experiment gave an alpha-particle yield per pulse of around 10^3 per steradian [5]. Recently, a much higher particle yield (around 10^7 per steradian) has been reported by using a more sophisticated experimental setup and similar laser intensity [6].

Our experiment aims to produce a high yield of alpha particles by triggering the proton (p)-boron (^{11}B) nuclear reaction:

$$^{11}\mathrm{B} + p \rightarrow 3\alpha + 8.7\ \mathrm{MeV}. \quad (1)$$

It is well known both from theoretical calculations and experimental measurements (performed with standard accelerators) that the reaction has a main channel with a maximum cross section for protons with energies of 600–700 keV [7–9]. Typically, this channel generates alpha particles with an energy distribution ranging from 2.5 to 5.5 MeV and a maximum at around 4.3 MeV (α_1). A secondary channel generating alpha particles in the energy range 6–10 MeV can also be present (α_2) [5,10,11].

II. METHODS

The experiment is performed at the Prague Asterix Laser System (PALS) facility in Prague [12], where a kJ-class (around 500 J in our experiment), subnanosecond (0.3-ns full width at half maximum, FWHM), linearly polarized laser is used to irradiate massive silicon targets. The laser pulse is focused in an 80-μm focal spot by an $f/2$ spherical lens to reach a nominal intensity of 3×10^{16} W cm^{-2} on the target surface in vacuum conditions of 10^{6}–10^{-5} mbar. The incidence angle between the laser-beam axis and the target normal is 30°. The nominal laser intensity is low compared with the high intensities achievable with picosecond and femtosecond laser systems. Nevertheless, recent experiments on laser-driven ion beams performed at PALS have shown maximum proton energies of a few MeV [13] which are typical for laser intensities of 5×10^{18}–10^{19} W cm^{-2} when shorter pulses are used [14].

Most of these targets were previously enriched with hydrogen and boron atoms through thermal annealing and

*Corresponding author.
picciotto@fbk.eu
†Corresponding author.
margaron@fzu.cz

50-keV ion-implantation doping processes performed at the Microtechnologies Laboratory (MTLab) at Fondazione Bruno Kessler in Trento [15,16]. Thus, well-known chemical-physical processes used in microelectronics help us to develop the idea of using boron-hydrogen-silicon targets for triggering a specific fusion reaction by precisely controlling the concentration and implantation or diffusion depth of the doping element. Here, we report mainly the results obtained by laser irradiation of massive silicon samples (0.5 mm thick) that are implanted with boron atoms (amu = 11) located at a depth of 190 nm and having a concentration of about 10^{22} cm^{-3}. (The boron layer is approximately 100 nm thick.) The concentration of hydrogen in the samples is increased through a thermal process where hydrogen atoms diffusing into the silicon matrix can link to it by forming Si-H bonds, which neutralize the silicon dangling bonds [17–20], thus reaching a concentration higher than 10^{20} cm^{-3}. Silicon samples where boron atoms are homogenously diffused into the substrate via the thermal annealing process (1 h at 1000 °C) are also fabricated and irradiated. In the latter case, the B atoms are distributed in a much thicker layer, starting from the sample surface up to a certain depth (>10 μm), resulting in lower local boron concentration (approximately 10^{20} cm^{-3}). These targets are irradiated in a series of measurements at the beginning of the experiment to be later compared with the results obtained with the implanted samples. Furthermore, silicon "pure" samples (not artificially hydrogenated and without boron doping) are also irradiated for comparison.

Ion analyzers, such as a Thomson-parabola (TP) spectrometer, time-of-flight (TOF) silicon-carbide (SiC) detectors [21–23], and solid-state nuclear-track detectors of PM-355 type [24,25], are used to detect and identify the produced proton and alpha-particle beams and measure their energy distribution in various directions with respect to the target normal. A detailed description of the experimental setup is sketched in Fig. 1(a).

The ns-long laser-pulse temporal shape is reported in Fig. 1(b). Although approximately 500 J are contained in the main pulse (0.3 ns at FWHM), the residual laser energy (about 100 J) is stored in the nanosecond pedestal. (Around 50 J of the pulse energy comes before the maximum-intensity peak is reached.) Figure 1(b) shows the presence of three intensity regions: 0-I represents the low-intensity (3×10^{10} W cm^{-2}) laser precursor, I-II is the high-intensity (10^{15} W cm^{-2}) prepulse, and II-III is the high-intensity (nominally 3×10^{16} W cm^{-2}) main pulse.

A series of hydrodynamic simulations is performed by using a 2D Prague Arbitrary Lagrangian-Eulerian (PALE) code [26]. This code employs the compatible staggered Lagrangian numerical scheme [27] and a rezoning or remapping mechanism improving the robustness of the simulations. Thermal conductivity is treated by a mimetic method with the standard Spitzer-Harm heat-conductivity coefficient and heat-flux limiter. Ray tracing is used for

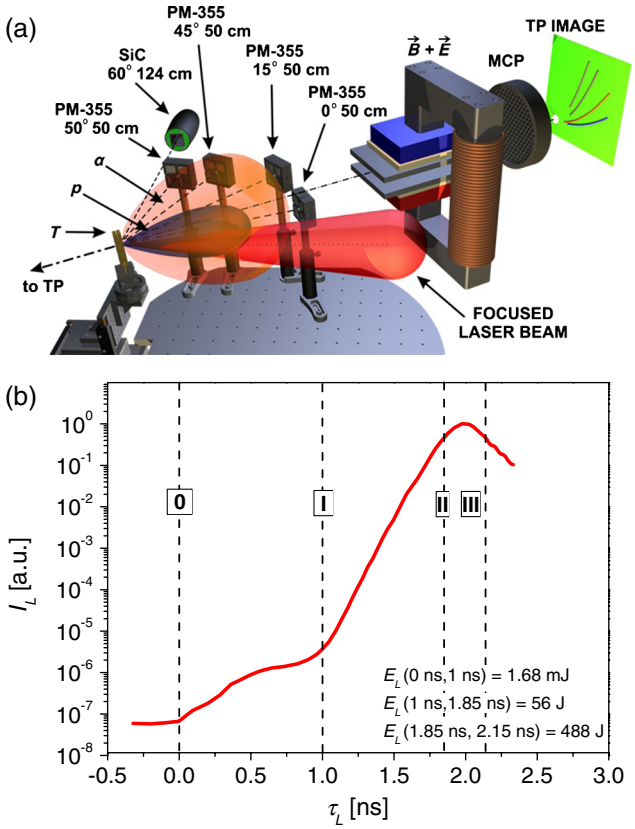

FIG. 1. (a) Experimental setup. T is the target, p is the proton beam, α is the alpha-particle beam, PM-355 is the nuclear-track detector, TP is the Thomson-parabola spectrometer, MCP is the microchannel plate, and SiC is the silicon-carbide detector. The angles are measured with respect to the target normal. (b) Laser intensity (I_L) against time (τ_L) in arbitrary units. The laser-energy content in different time windows is reported in the legend.

laser-absorption modeling. The simulations shown in this paper are performed in the Lagrangian regime; thus, the layers of the targets remain separated throughout the whole simulation. The initial computational mesh is adjusted to the layered targets using a finer mesh resolution at the target surface. The simulations are stopped after 1.85 ns [see Fig. 1(b) as a reference]. The simulations are performed by considering different target geometries: (a) a B-implanted layer in a Si substrate with the above-described characteristics, (b) a B-diffused layer in a Si substrate with the above-described characteristics, and (c) a B layer deposited on a Si-substrate surface with the same atomic concentration as in (a). The comparison of the hydrodynamic simulations corresponding to these three different geometries is shown in Fig. 2, where z is the plasma-expansion longitudinal direction (parallel to the target normal) and r is the plasma-expansion transverse direction (parallel to the target surface). The simulations take into account the time evolution of the laser pulse in the range 1–1.85 ns. It is clearly shown that after 1.85 ns, the B plasma is better confined (200 μm from the target surface) and has a

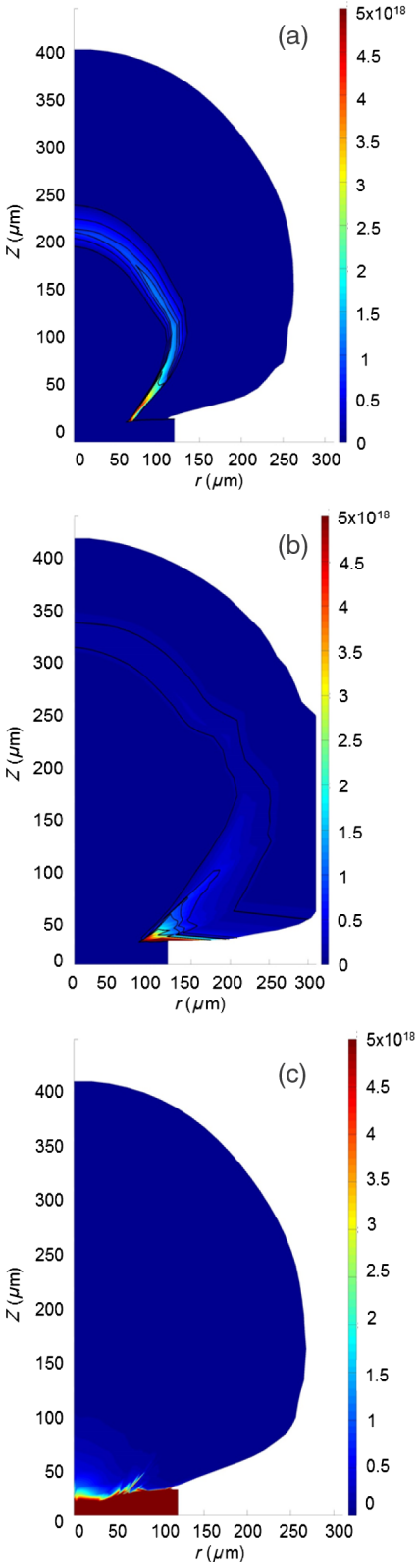

FIG. 2. 2D PALE hydrodynamic simulations of the boron-plasma expansion after the action of the laser pulse (in the range 1–1.85 ns) for (a) the B layer implanted in the SiH substrate, (b) the B layer deposited on the SiH substrate, and (c) the B layer diffused in the SiH substrate. The gradient scale on the right-hand side shows the B-plasma density.

higher density (approximately 10^{18} cm^{-3}) in (a) than in (b) and (c). Thus, in (a), the accelerated protons can subsequently interact with higher-density plasma and have a higher probability to induce nuclear reactions than in (b) and (c).

III. EXPERIMENTAL RESULTS

To give clear-cut evidence of alpha-particle generation, the PM-355 nuclear-track detectors [previously calibrated by using monoenergetic ions provided by a standard accelerator, as shown in Fig. 3(e)] are placed at a distance of about 50 cm from the target surface and at different angles (from 0° to 50° with respect to the target normal) and covered by aluminum foils of different thicknesses (6–30 μm) to filter low-energy plasma ions out and to avoid overlapping among neighboring ion tracks. Figure 3(a) shows a typical PM-355 snapshot where craters induced by alpha particles (large dark craters) and by protons (small light craters) passing through the Al foil of 15 μm in thickness are clearly distinguished when boron-implanted hydrogenated silicon (Si-H-B) samples are irradiated. The corresponding track-diameter distribution is shown in Fig. 3(b). B-diffused silicon samples (described in Sec. II) are irradiated; nevertheless, a much lower flux of alpha particles is measured (1×10^4 cm^{-2} in comparison to 3×10^6 cm^{-2} obtained with the B-implanted samples), in agreement with qualitative expectations based on the hydrodynamic simulation results (see Fig. 2). Pure silicon samples (Si) are also irradiated for comparison, and only proton-generated craters are distinguishable on the PM-355 detectors, as demonstrated by the typical snapshot and corresponding track-diameter distribution shown in Figs. 3(c) and 3(d), respectively. The calibration of PM-355 detectors used in our experiment is shown in Fig. 3(e).

The method of differential energy filtering of ions, which induces tracks in calibrated PM-355 detectors, allows us to determine their energy distribution, reported in Fig. 4(a). The energy of alpha particles ranges from 4 to 8 MeV with a maximum at around 4.5 MeV, which is in agreement with the expected values from the nuclear-fusion reaction [5–11], although a more precise estimation of the energy distribution has been performed through TOF measurements by the SiC detector.

The presence of B ions in the nuclear-track detectors is excluded since Al filters with up to 20-μm thickness are used. The energy that potential B ions would need to pass through such filters is about 20 MeV, i.e., about 2 MeV/u, thus well above the typical values reported in several papers (e.g., Ref. [28]), indicating a maximum energy of around 300 keV with a laser irradiance of about 5×10^{16} W μm^2 cm^{-2}. Even assuming effective laser irradiance being around 10^{18} W μm^2 cm^{-2}, the corresponding B-ion energy should not exceed 1 MeV/u [28]. Moreover, if one looks carefully at the ion TOF spectrum later described in Fig. 6 and at the TP

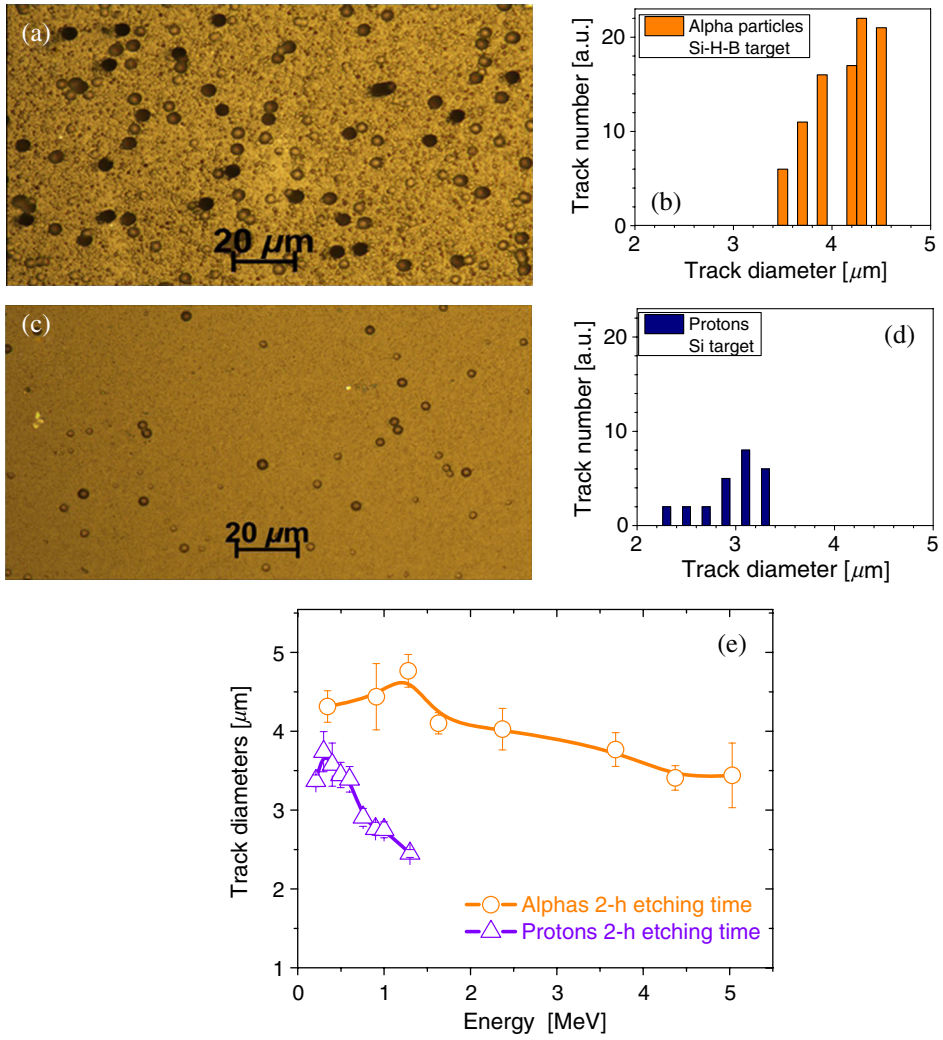

FIG. 3. PM-355 film snapshot showing craters produced by incident protons (small light craters) and alpha particles (large black craters) for (a) the Si-H-B target and (b) the corresponding histograms of particle crater diameters. (c) The PM-355 snapshot shows craters produced by incident protons (small light craters) for the Si target and (d) corresponding histograms of particle crater diameters. (e) The PM-355 calibration curve for alpha particles and protons after 2-h etching time. An Al foil of 15 μm in thickness is placed in front of the PM-355 films.

proton-energy spectrum in Fig. 7(b), it is evident that the alpha-one and alpha-two peaks cannot be correlated to the arrival of plasma ions. In fact, the maximum proton energy registered by our TP spectrometer is about 1 MeV, and typically, in a plasma expansion, other ions will acquire a lower energy per nucleon compared to protons. Thus, the TOF spectrum cannot show plasma ions (e.g., protons, Si ions, B ions) reaching the detector in a time shorter than 90 ns, which is also evident from the TOF spectrum reported in Fig. 6, where the peaks at 60 and 80 ns correspond to the two channels of the fusion reaction (also confirmed by the typical energy distribution reported in the literature [5]). Further "spurious effects," e.g., beam-fusion reactions induced by plasma B ions hitting the detector surface, are also excluded since our detectors are placed at different angles (see Fig. 1), including large ones (e.g., 60°) with respect to the target normal, where plasma-ion emission is very limited. In fact, it is well known that laser-driven ion sources expand mainly along the target normal within a cone usually not larger than 30°–40° [29].

The PM-355 detectors placed at different angles allow determining the alpha-particle angular distribution. This distribution shows a maximum yield of about 10^9 particles per steradian, as reported in Fig. 4(b). The estimated total number of alpha particles produced per laser pulse is about 4×10^8. The total number of alpha particles produced is about 2×10^3 times higher than previous results in a similar laser-irradiation geometry reported in Ref. [5] (considering the actual yield suggested in Ref. [30]) when using a 1.5-ps laser system at an intensity of 2×10^{18} W cm^{-2}, thus suggesting that our experimental scheme and target geometry provide an extremely high-efficiency nuclear reaction. An alpha-particle yield of about 10^7 per steradian has been recently reported by Labaune *et al.* by using a more

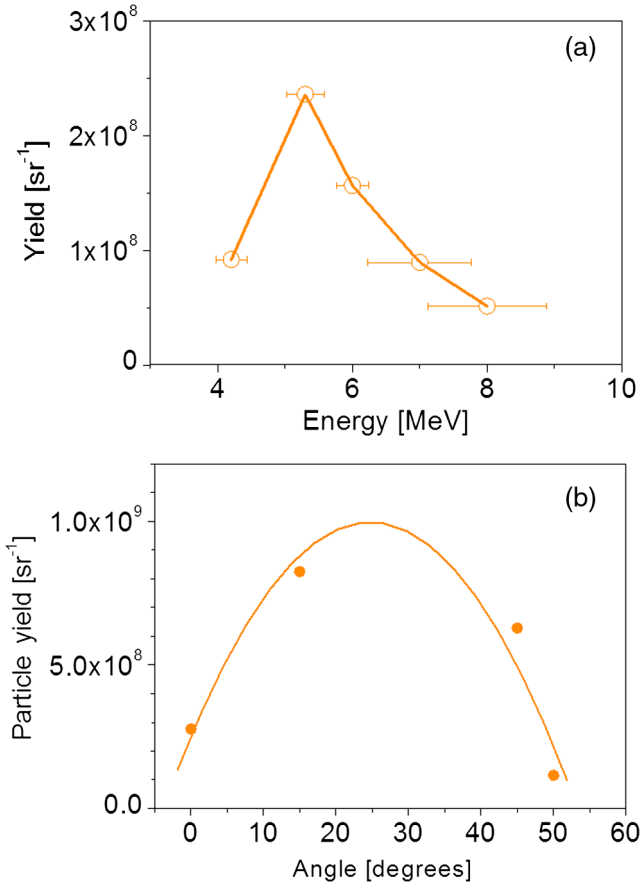

FIG. 4. (a) Alpha-particle energy distribution obtained from PM-355 analysis using detectors with different Al filter thicknesses (6–20 μm) and placed at an angle of about 45° with respect to the laser-incident direction in the same laser shot. (b) Alpha-particle angular distribution obtained from PM-355 analysis using detectors placed at different angles with respect to the laser-incident direction in the same laser shot.

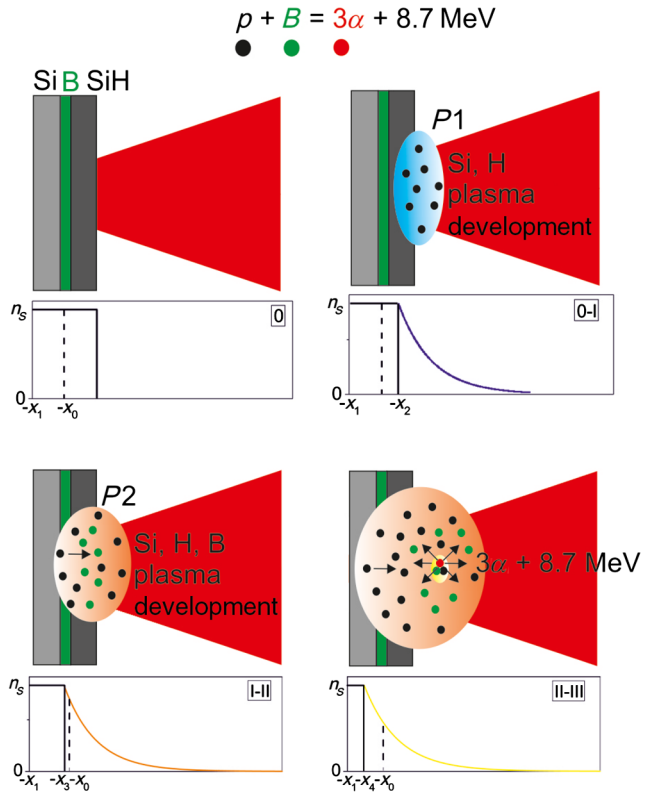

FIG. 5. Laser-target, laser-plasma, and proton-boron interactions in the 2-ns range before the maximum laser intensity [0-III in Fig. 1(b)]: n_s is the solid density, 0 is the target surface position, x_0 is the depth of the boron atoms, x_1 is the substrate extension, x_2, x_3, and x_4 are the ablation depths at three given times, and $P1$ and $P2$ are plasmas generated by the laser pulse in the 0-I and I-II regions, respectively.

sophisticated experimental setup with two laser beams (ns and ps) and two different targets [6]. Nevertheless, our results show an increase by a factor 10^2 of the number of alpha particles (around 10^9 per steradian in our case) by using a longer laser pulse (ns) with a low contrast and a maximum nominal laser intensity about 10^2 times lower (3×10^{16} W cm^{-2}) than in Ref. [6].

IV. DISCUSSIONS

Our proposed mechanism describing a simplified picture of the long laser-pulse interaction with the H-enriched and B-doped silicon target (Si-H-B) is sketched in Fig. 5. At a time of 2 ns before the maximum intensity, the laser pulse starts to interact with the Si-H layer causing ablation and ionization of the target material during the 0-I period (the laser fluence is about 30 J cm^{-2}, i.e., well above the ablation threshold for Si [31]), thus sweeping away the Si-H layer on the target surface. The target ablation continues during the I-II period affecting the implanted boron layer, as clearly demonstrated by the hydrodynamic simulations shown in Fig. 2. In fact, the ablation depth numerically estimated at the end of this period [corresponding to 1.85 ns in Fig. 1(b)] is around 10 μm; thus, the B plasma has clearly developed [see Fig. 2(a)] and protons are already accelerated from the Si-H inner layer. This process might also benefit from the self-focusing mechanism initiated by the laser beam interacting with the plasma medium, which causes a change in the refractive index (with the power of the laser pulse being higher than the threshold for relativistic self-focusing [32,33]). Thus, the effective laser intensity might be higher than the nominal one, causing a corresponding increase in the plasma temperature. However, the relatively high proton energy measured in our experiment could also be the result of an efficient acceleration process that benefits from the long laser-pulse width (nanoseconds) [34]. In the II-III period, the protons accelerated backward catch the B ions and the "beam-target" nuclear reaction occurs. In fact, the B ions can be assumed to be at rest since the proton velocity is about 1×10^7 m/s and the boron-plasma one is about 2×10^6 m/s. Our theoretical model is simplified since the involved processes are dynamic, and there is a

clear interplay between the B-plasma density (hence, the distance of the B-ion cloud from the target surface) and the proton-beam energy.

As previously demonstrated experimentally and confirmed throughout our campaign, the accelerated protons have a wide energy distribution with a typical cutoff at about 2 MeV [13,29]. Such a maximum proton energy is compatible with a laser intensity of 5×10^{18}–10^{19} W cm^{-2} when using shorter laser pulses [14]. The number of protons accelerated backward when irradiating a hydrogenated silicon target (equivalent to the Si-H substrate in our Si-H-B geometry) is about 10^{11}, as measured in our previous work [29].

The energy distribution of protons, as well as alpha particles, is observed far from the irradiated target by two additional diagnostics: the silicon-carbide detector (in TOF geometry) and the Thomson-parabola spectrometer, as depicted in Fig. 1(a). They are both real-time devices that allow us to obtain a preliminary response during the experimental measurements, which has been later on confirmed by the *ex situ* data measured with the PM-355 detectors. In addition, they provide a full-range energy distribution with a much higher energy resolution than the previous technique using PM-355 detectors, which was nevertheless fundamental for estimating the absolute number of produced particles.

A typical signal of the SiC detector screened from low-energy plasma ions with an 8-μm aluminum foil is shown in Fig. 6. Since the SiC detector is placed at an angle of 65° with respect to the target-normal direction, the yield of plasma ions impinging onto it is strongly reduced. Because of the subnanosecond response and the high signal-to-noise ratio of the SiC detector, this TOF spectrum clearly shows three ion peaks: the alpha particles coming from the $^{11}\mathrm{B}(p,\alpha)2\alpha$ reaction main channel (α_1) and arriving at about 80 ns, the alpha particles produced within the secondary channel (α_2) at about 60 ns, and the proton-ion beam accelerated in the plasma and expanding backward at about 105 ns. The alpha-particle energy distribution can easily be retrieved from the TOF signal [35].

The α_1 signal shows particles with energies ranging from 3 to 8 MeV (centered at 4.6 MeV and with an approximately 40% energy spread at FWHM) and the α_2 distribution from 7 to 11 MeV (centered at 8.9 MeV with an approximately 25% energy spread at FWHM), in agreement with experimental data in the literature [5,8]. Results obtained with a Si target are also shown in the plot of Fig. 6(a) for comparison. The absence of the peaks corresponding to alpha particles from the nuclear reaction is evident, while a low signal ascribable to plasma protons and heavier ions (probably Si) is observed starting from approximately 80 ns.

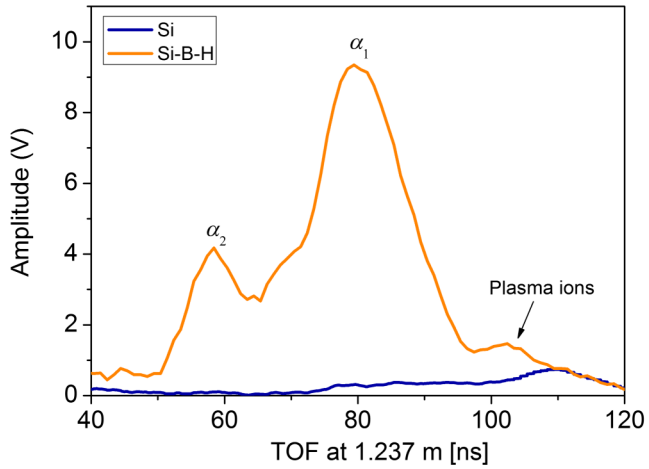

FIG. 6. Ion TOF distribution for the Si-H-B target (orange curve) with the alpha-particle signal (α_1 and α_2) and plasma ions measured by the SiC detector covered by a 8-μm aluminum foil and placed at 65° with respect to the target normal. The ion TOF distribution for the Si target (blue curve) showing the presence of only plasma ions (no fusion event has occurred) is also reported for comparison.

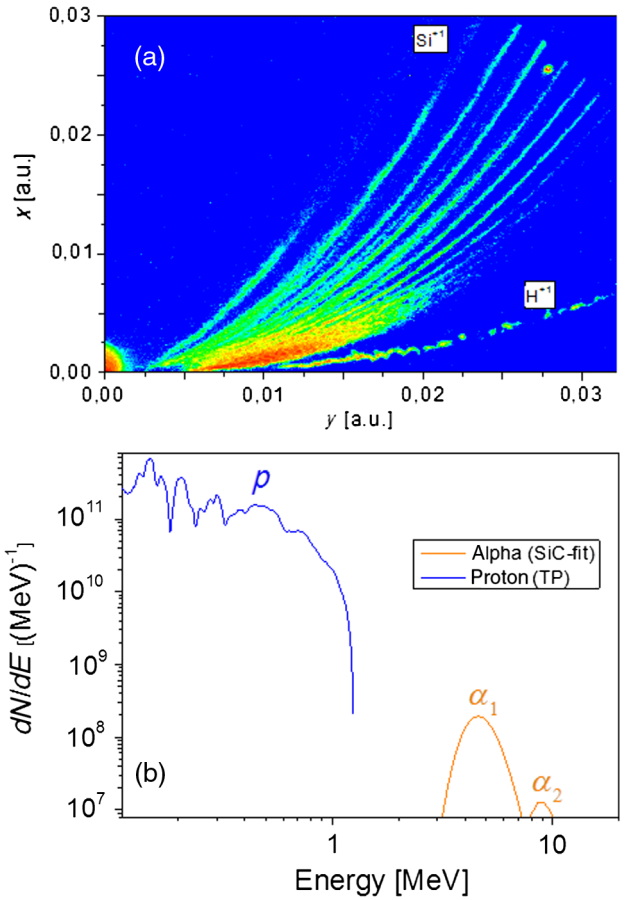

FIG. 7. (a) Typical TP spectrometer snapshot showing the presence of backward-accelerated protons and heavier plasma ions (a). The corresponding proton-energy distribution and the comparison with the alpha-particle one (obtained by fitting the TOF spectrum in Fig. 6) are shown in (b).

The TP spectrometer allows determining the energy distribution of protons propagating backward (also detected with PM-355 films), showing a maximum value of about 1 MeV and a relative maximum (wide plateau) between 200 and 700 keV, i.e., covering the region where the cross section of the nuclear reaction is maximized [7]. A TP snapshot and the corresponding proton-energy distribution are shown in Figs. 7(a) and 7(b), respectively. The other ion-energy distributions (including the alpha-particle ones) are not estimated by the TP because of the overlapping between neighboring parabolas (i.e., low spatial resolution).

V. CONCLUSIONS

We have experimentally demonstrated the possibility of enhancing the $^{11}\mathrm{B}(p,\alpha)2\alpha$ fusion reaction induced by high-intensity laser pulses interacting with solid targets. A fusion rate of about 10^9 alpha particles per steradian per pulse was achieved by using low-contrast, long laser pulses and advanced targets. The high-current proton beam generated by the long (nanosecond) laser pulse presented an optimal energy distribution with a plateau around the maximum of the nuclear-reaction cross section. Furthermore, the multilayer target geometry with a high boron concentration at a given depth of the hydrogenated silicon sample allowed the nuclear reaction to occur when the boron-ion density was still very high (i.e., still close to the target surface), thus ensuring a very high-fusion rate. The protons accelerated from the Si-H substrate that propagate backward (against the laser-pulse propagation) are responsible for the nuclear reaction; in fact, they can easily catch the whole blowoff B plasma (having a similar divergence) also expanding backward but with lower velocity.

Various possibilities for a further enhancement of this (or similar) aneutronic nuclear-fusion reactions can be investigated analytically, numerically, and experimentally through the optimization of both laser characteristics (nanosecond pulse shape, contrast, and energy) and target geometry (the available silicon microtechnology can offer a wide range of configurations), which, in turn, might allow the generation of new brilliant ultraclean radiation sources reducing problems associated with neutron emission, e.g., activation, radiation damage, shielding, and other safety issues. Such radiation sources can be attractive not only for their potential use in the generation of fusion energy (in this case, the proposed scheme will have to be modeled and scaled up to conditions relevant to future experimental investigations with large-scale laser facilities based on inertial confinement fusion) but also for the generation of high-directionality, high-current, quasimonoenergetic ion beams (the measured α_2 average energy was about 9 MeV with a 25% energy spread) at moderate laser intensity through very compact systems that can be alternative to standard accelerators.

The scientific advance of our experimental results is not only connected to the very high alpha-particle yield but also to the use of a moderate laser power (2 TW) and intensity (3×10^{16} W/cm^2), which enable future possibilities to use compact laser systems (for instance, based on newly established diode-pumped laser technology) and simple irradiation geometries (single laser and single target). In fact, the moderate laser power allows the use of a long laser pulse, which does not imply special laser techniques for compressing the pulse (e.g., chirped pulse amplification) and, thus, a less sophisticated (and cheaper) system. In fact, such relatively long pulses do not need to be transported in vacuum since the laser fluence is below the threshold for laser-induced breakdown sparks in air. Moreover, since the laser intensity is moderate, the spot size on target can be much higher than the diffraction limit, thus allowing us to generate a high-yield B plasma, thanks to volumetric effects, which, in turn, increase the number of fusion events.

Moreover, our hydrodynamic simulations suggest that the relevant physical mechanisms that enable the beam-target fusion reaction occur in a temporal window preceding the main peak of the laser pulse. In fact, the numerically estimated B-plasma density value drops below 10^{18} cm^{-3} after 1.85 ns; hence, the number of alpha particles generated from the fusion reaction decreases drastically before the main laser-peak intensity is reached on target. Thus, in principle, only a small part of the laser energy (approximately 50 J) is used for realizing the nuclear reaction, which implies the future possibility to realize this experiment using small and cost-effective laser systems. Such compact systems (tens of joules, nanosecond class, and high repetition rate), for instance, based on newly established diode-pumped laser technology, can allow us to increase the efficiency of this mechanism as well as the compactness of the whole experimental setup.

ACKNOWLEDGMENTS

The authors thank the technical personnel C. Gazzin and S. Tomasi of the Microelectronic Laboratory of Fondazione Bruno Kessler for their support during ion implantation of the samples and also R. Dudzak, M. Pfeifer, J. Skala, and the technical personnel of the PALS laboratory for their support during the experimental work; C. Lanzieri, S. Masci, L. Martinelli, and D. Puglisi for their collaboration in SiC detector manufacturing and assembling; and S. V. Bulanov and O. Klimo for the scientific discussions and suggestions. M. K. was supported in part by the Czech Ministry of Education, Youth and Sports through the COST Project No. LD14089. Moreover, this research was supported by the CHARPAC Work Package of the Laserlab-Europe III (Project No. 284464), by the Ministry of Education, Youth and Sports of the Czech Republic (ELI-Beamlines Registered No. CZ.1.05/1.1.00/02.0061 and PALS Project Registered No. LM2010014), and by the Academy of Sciences of the Czech Republic (M100101210).

[1] M. L. E. Oliphant and L. Rutherford, *Experiments on the Transmutation of Elements by Protons*, Proc. R. Soc. A **141**, 259 (1933).

[2] G. L. Kulcinski and J. F. Santarius, *Nuclear Fusion: Advanced Fuels under Debate*, Nature (London) **396**, 724 (1998).

[3] H. Hora, G. H. Miley, M. Ghoranneviss, B. Malekynia, N. Azizi, and X. T. He, *Fusion Energy without Radioactivity: Laser Ignition of Solid Hydrogen–Boron (11) Fuel*, Energy Environ. Sci. **3**, 479 (2010).

[4] N. Rostoker, M. W. Binderbauer, and H. J. Monkhorst, *Colliding Beam Fusion Reactor*, Science **278**, 1419 (1997).

[5] V. S. Belyaev, A. P. Matafonov, V. I. Vinogradov, V. Krainov, P. Lisitsa, V. S. Roussetski, A. S. Ignatyev, G. N. Andrianov, *Observation of Neutronless Fusion Reactions in Picosecond Laser Plasmas*, Phys. Rev. E **72**, 026406 (2005).

[6] C. Labaune, S. Depierreux, C. Goyon, G. Loisel, V. Yahia, and J. Rafelski, *Fusion Reactions Initiated by Laser-Accelerated Particle Beams in a Laser-Produced Plasma*, Nat. Commun. **4**, 2506 (2013).

[7] W. M. Nevins and R. Swain, *The Thermonuclear Fusion Rate Coefficient for* $p-{}^{11}\mathrm{B}$ *Reactions*, Nucl. Fusion **40**, 865 (2000).

[8] D. C. Moreau, *Potentiality of the Proton-Boron Fuel for Controlled Thermonuclear Fusion*, Nucl. Fusion **17**, 13 (1977).

[9] S. Stave, M. W. Ahmed, R. H. France III, S. S. Henshaw, B. Muller, B. A. Perdue, R. M. Prior, M. C. Spraker, and H. R. Weller, *Understanding the* $^{11}\mathrm{B}(p,\alpha)\alpha\alpha$ *Reaction at the 0.675 MeV Resonance*, Phys. Lett. B **696**, 26 (2011).

[10] H. W. Becker, C. Rolfs, and H. P. Trautvetter, *Low-Energy Cross Sections for* $^{11}\mathrm{B}(p,3e)^{*}$, Z. Phys. A **327**, 341 (1987).

[11] V. F. Dmitriev, *α-Particle Spectrum in the Reaction* $p+{}^{11}\mathrm{B}\rightarrow\alpha+{}^{8}\mathrm{B}e^{*}\rightarrow 3\alpha$, Phys. At. Nucl. **72**, 1165 (2009).

[12] K. Jungwirth, A. Cejnarova, L. Juha, B. Kralikova, J. Krasa, E. Krousky, P. Krupickova, L. Laska, K. Masek, T. Mocek, M. Pfeifer, A. Präg, O. Renner, K. Rohlena, B. Rus, J. Skala, P. Straka, and J. Ullschmied, *The Prague Asterix Laser System*, Phys. Plasmas **8**, 2495 (2001).

[13] D. Margarone, J. Krasa, L. Laska, A. Velyhan, T. Mocek, J. Prokupek, E. Krousky, M. Pfeifer, S. Gammino, L. Torrisi, J. Ullschmied, and B. Rus, *Measurements of the Highest Acceleration Gradient for Ions Produced with a Long Laser Pulse*, Rev. Sci. Instrum. **81**, 02A506 (2010).

[14] K. Krushelnick, Z. Najmudin, and A. E. Dangor, *Particle Acceleration Using Intense Laser Produced Plasmas*, Laser Phys. Lett. **4**, 847 (2007).

[15] A. Picciotto, D. Margarone, J. Krasa, A. Velyhan, E. Serra, P. Bellutti, G. Scarduelli, L. Calliari, E. Krousky, B. Rus, and M. Dapor, *Laser-Driven Acceleration of Protons from Hydrogenated Annealed Silicon Targets*, Europhys. Lett. **92**, 34 008 (2010).

[16] A. Picciotto, D. Margarone, M. Crivellari, P. Bellutti, S. Colpo, L. Torrisi, J. Krasa, A. Velhyan, and J. Ullschmied, *Microfabrication of Silicon Hydrogenated Thin Targets for Multi-MeV Laser-Driven Proton Acceleration*, Appl. Phys. Express **4**, 126401 (2011).

[17] K. J. Chang and D. J. Chadi, *Hydrogen Bonding and Diffusion in Crystalline Silicon*, Phys. Rev. B **40**, 11 644 (1989).

[18] S. Arrhenius, *Über die Reaktionsgeschwindigkeit bei der Inversion von Rohrzucker durch Säuren*, Z. Naturforsch. Teil A **4**, 226 (1889).

[19] A. Van Wieringen, and N. Warmoltz, *On the Permeation of Hydrogen and Helium in Single Crystal Silicon and Germanium at Elevated Temperatures*, Physica (Amsterdam) **22**, 849 (1956).

[20] A. Fick, *On Liquid Diffusion*, Philos. Mag. **10**, 30 (1855).

[21] D. Margarone *et al.*, *New Methods for High Current Fast Ion Beam Production by Laser-Driven Acceleration*, J. Appl. Phys. **109**, 103302 (2011).

[22] G. Bertuccio, D. Puglisi, L. Torrisi, and C. Lanzieri, *Silicon Carbide Detector for Laser-Generated Plasma Radiation*, Appl. Surf. Sci. **272**, 128 (2013).

[23] G. Bertuccio, *Silicon Carbide Radiation Microdetectors for Harsh Environments*, Proc. SPIE Int. Soc. Opt. Eng. **7679**, 76790T (2010).

[24] A. Szydłowski, A. Malinowska, T. Czyżewski, I. Fijał, M. Jaskóła, A. Korman, M. J. Sadowski, and W. Kretschmer, *Advantage of PM-355 Nuclear Track Detector in Light-Ion Registration and High-Temperature Plasma Diagnostics*, Radiation Measurements **34**, 325 (2001).

[25] A. Malinowska, A. Szydłowski, M. Jaskoła, A. Korman, K. Malinowski, and M. Kuk, *Calibration of New Batches and a Study of Applications of Nuclear Track Detectors under the Harsh Conditions of Nuclear Fusion Experiments*, Nucl. Instrum. Methods Phys. Res., Sect. B **281**, 56 (2012).

[26] R. Liska, M. Kucharik, J. Limpouch, O. Renner, P. Vachal, L. Bednarik, and J. Velechovsky, *ALE Method for Simulations of Laser-Produced Plasmas*, Springer Proc. Math. **4**, 857 (2011).

[27] E. J. Caramana, D. E. Burton, M. J. Shashkov, and P. P. Whalen, *The Construction of Compatible Hydrodynamics Algorithms Utilizing Conservation of Total Energy*, J. Comput. Phys. **146**, 227 (1998).

[28] S. J. Gitomer, *Fast Ions and Hot Electrons in the Laser-Plasma Interaction*, Phys. Fluids **29**, 2679 (1986).

[29] D. Margarone, J. Krasa, A. Picciotto, L. Torrisi, L. Laska, A. Velyhan, J. Prokupek, L. Ryc, P. Parys, J. Ullschmied, and B. Rus, *High Current, High Energy Proton Beams Accelerated by a Sub-nanosecond Laser*, Nucl. Instrum. Methods Phys. Res., Sect. A **653**, 159 (2011).

[30] S. Kimura, A. Anzalone, and A. Bonasera, *Comment on "Observation of Neutronless Fusion Reactions in Picosecond Laser Plasmas"*, Phys. Rev. E **79**, 038401 (2009).

[31] A. V. Bulgakov, I. Ozerov, and W. Marine, *Cluster Emission under Femtosecond Laser Ablation of Silicon*, Thin Solid Films **453–454**, 557 (2004).

[32] G. Sun, E. Ott, Y. C. Lee, and P. Guzdar, *Self-Focusing of Short Intense Pulses in Plasmas*, Phys. Fluids **30**, 526 (1987).

[33] L. Torrisi, D. Margarone, L. Laska, J. Krasa, A. Velyhan, M. Pfeifer, J. Ullschmied, and L. Ryc, *Self-Focusing Effect in Au-Target Induced by High Power Pulsed Laser at PALS*, Laser Part. Beams **26**, 379 (2008).

[34] P. Mora, *Plasma Expansion into a Vacuum*, Phys. Rev. Lett. **90**, 185002 (2003).

[35] J. Krasa, *Gaussian Energy Distribution of Fast Ions Emitted by Laser-Produced Plasmas*, Appl. Surf. Sci. **272**, 46 (2013).